IEICE TRANS. ELECTRON., VOL.E92–C, NO.7 JULY 2009

INVITED PAPER *Special Section on Recent Advances in Ultra-high-speed Photonic Devices for Next-generation Optical Fiber Communications*

High Speed 1.1-μm-Range InGaAs-Based VCSELs

Naofumi SUZUKI[†a)], **Takayoshi ANAN**[†], ***Nonmembers***, **Hiroshi HATAKEYAMA**[†], **Kimiyoshi FUKATSU**[†], **Kenichiro YASHIKI**[†], ***Members***, **Keiichi TOKUTOME**[†], **Takeshi AKAGAWA**[†], ***and*** **Masayoshi TSUJI**[†], ***Nonmembers***

SUMMARY We have developed InGaAs-based VCSELs operating around 1.1 μm for high-speed optical interconnections. By applying GaAsP barrier layers, temperature characteristics were considerably improved compared to GaAs barrier layers. As a result, 25 Gbps 100°C error-free operation was achieved. These devices also exhibited high reliability. No degradation was observed over 3,000 hours under operation temperature of 150°C and current density of 19 kA/cm^2. We also developed VCSELs with tunnel junctions for higher speed operation. High modulation bandwidth of 24 GHz and a relaxation oscillation frequency of 27 GHz were achieved. 40 Gbps error-free operation was also demonstrated.

key words: *vertical-cavity surface-emitting lasers (VCSELs), optical interconnections, semiconductor lasers, tunnel junction, high-speed modulation*

1. Introduction

Vertical-cavity surface-emitting lasers (VCSELs) have been used as light sources for such short-distance optical communications as Giga-bit Ethernet or fiber channel systems. Their modulation speeds have been improved and those for 10 Giga-bit Ethernet are now commercially available. Recently, however, higher modulation speed has grown in demand for optical interconnections in high-end computing systems or next-generation data-communication networks. In these applications, transmission speed higher than 20 Gbps is required. So far, high-speed VCSELs operating at 0.85 μm have been developed and high modulation bandwidths up to 21.5 GHz have been reported [1]–[4]. These VCSELs have active layers consisting of GaAs/AlGaAs quantum wells (QWs). On the other hand, in general, higher speed operation of semiconductor lasers requires higher current density, which results in shorter device lifetime. Consequently, there is a trade-off between speed and reliability [5]. To ameliorate the trade-off and achieve high speed operation and high reliability simultaneously, InGaAs/GaAs QWs are suitable for active layers of VCSELs. The high differential gains of the quantum wells are preferable for high speed operation [6]. Actually, the quantum wells were used as active layers of 1.1-μm-range laser diodes and achieve bandwidth as high as 40 GHz [7]. This material system has also been used as an active layer of 0.98-μm laser diodes for EDFA excitation and exhibits excellent reliability. This is thought to be attributed to the fact that the indiums in the wells suppress dislocation motion [8]. In a previous paper, we described 1.1-μm-range VCSELs with InGaAs/GaAs MQWs as active layers. High modulation bandwidth of 20 GHz and 30 Gbps 100 m transmission were demonstrated [9]. Another group also reported high speed operation up to 35 Gbps with small-aperture 0.98 μm InGaAs VCSELs [10]. These high-speed operations were achieved under room temperature. For practical use, however, operations under a wide temperature range are necessary. Meanwhile, higher speed operations are also desired for such applications as light sources of very short reach in 40 Gbps communication systems.

For high temperature operation, we have developed VCSELs with InGaAs/GaAsP quantum wells as active layers. By applying GaAsP barrier layers, temperature characteristics were considerably improved compared to GaAs barrier layers. We have also developed tunnel junction VCSELs for higher speed operation. Record-high modulation bandwidth of 24 GHz and error-free operation up to 40 Gbps were achieved.

2. Oxide-Confined VCSELs with SC-MQWs

2.1 GaAsP Barrier Layer

From the viewpoint of reducing costs and power consumption of optical transmitters, uncooled operations of light sources under a wide temperature range are desirable. For higher temperature operation, it is effective to increase conduction-band-offset between well and barrier layers, which suppress carrier overflow. The conduction-band-offset can be increased by changing barrier layers. There were two alternatives for the barrier layers, which were AlGaAs and GaAsP. We chose GaAsP because it has opposite strain from the InGaAs layer. Thus, QWs are a so-called strain-compensated (SC) structure, which can suppress generation of misfit dislocations and improve reliability. This effect cannot be achieved with AlGaAs, which has the same strain as InGaAs.

Figure 1 shows average strain of the $In_{0.3}Ga_{0.7}As/GaAs_{1-x}P_x$ triple quantum wells and critical thickness that was calculated based on Matthews-Blakeslee theory [11]. The thicknesses of the well and barrier layers were 5 and 10 nm, respectively. With phosphorous composition of 0.2, the net strain can be suppressed sufficiently. By using $GaAs_{0.8}P_{0.2}$ as the barrier layer, conduction-band-offset can be increased by 100 meV compared to the GaAs barrier

Manuscript received November 5, 2008.
Manuscript revised January 9, 2009.

[†]The authors are with Nano-Electronics Res. Labs., NEC Corporation, Otsu-shi, 520-2141 Japan.
a) E-mail: n-suzuki@dh.jp.nec.com

DOI: 10.1587/transele.E92.C.942

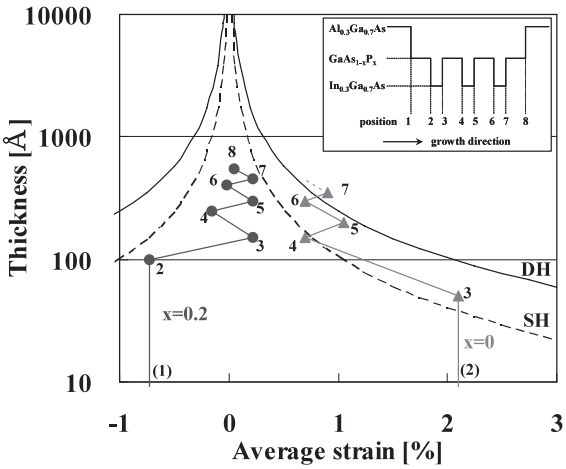

Fig. 1 Average strain of the $In_{0.3}Ga_{0.7}As/GaAs_{1-x}P_x$ quantum wells (QWs) and critical thickness. The inlet shows schematic energy band diagram of the QWs. Each point in the graph shows the average strain during growth. The numbers beside the points indicate the position in the QWs, which are shown in the inlet. DH and SH mean double hetero structure and single hetero structure, respectively.

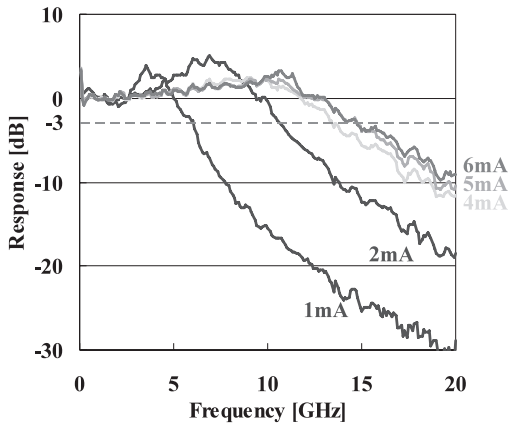

Fig. 2 Small signal modulation response of the VCSEL with $In_{0.3}Ga_{0.7}As/GaAs_{0.8}P_{0.2}$ QWs active layer at a temperature of 100°C.

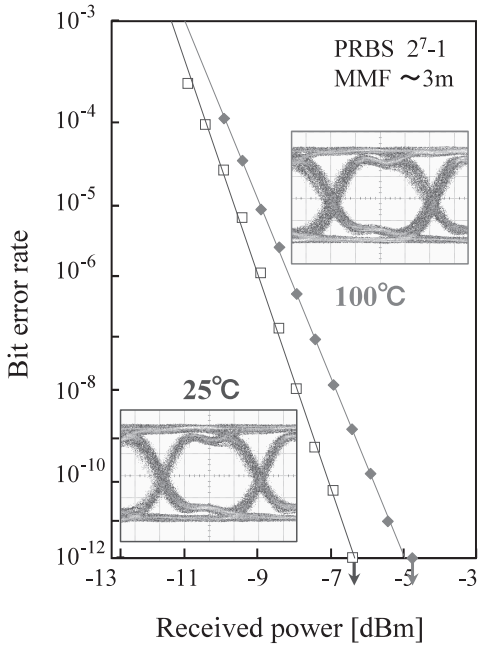

Fig. 3 Measured eye diagrams and bit error rates under 25 Gbit/s transmission rate at 25°C and 100°C.

layer [12].

2.2 Device Structure

We fabricated oxide-confined VCSELs with three $In_{0.3}Ga_{0.7}As/GaAs_{0.8}P_{0.2}$ SC-QWs as active layers. The top and bottom mirrors consisted of 23 pairs of p-$Al_{0.12}Ga_{0.88}As/Al_{0.9}Ga_{0.1}As$-DBR and 33.5 pairs of $GaAs/Al_{0.9}Ga_{0.1}As$-DBR, respectively. The top DBR included an $Al_{0.98}Ga_{0.02}As$ oxidation layer with a thickness of 30 nm. A dry-etched mesa with a 27-μm diameter had an oxide aperture with around a 6-μm diameter. A proton-implantation was applied to the mesa avoiding the center region of 15 μm, which reduced capacitance of the mesa from around 0.3 pF to 0.1 pF.

2.3 Characteristics

We estimated maximum lasing temperature (T_{max}) of the device as a barometer of temperature characteristics by extrapolation of the relations between maximum powers and temperatures. Maximum lasing temperature as high as 219°C was estimated. The high T_{max} value was obtained without large offset between gain peak and lasing wavelength [13], which means the VCSELs will work over a wide temperature range.

Next, we evaluated modulation characteristics of the device under high temperature. Figure 2 shows small signal modulation responses at 100°C. A wide 3 dB-bandwidth of about 15 GHz under a bias current of 6 mA was achieved. Figure 3 shows measured eye diagrams and bit error rate (BER) characteristics at 25°C and 100°C. The bit rate was 25 Gbit/s with a pseudorandom bit sequence of $2^7 - 1$ word length. A high-speed multimode receiver with a 3-dB bandwidth of 20 GHz, which consisted of PIN-PD and TIA [9], was used for signal detection. The modulation voltage was 0.6 $V_{p\text{-}p}$ and the bias current was 6 mA. Clear eye openings and error-free operations (BER$< 10^{-12}$) were successfully demonstrated even under temperature as high as 100°C.

2.4 Reliability

We evaluated reliability of the VCSELs with SC-MQWs. Figure 4 shows the output power variations of 45 devices during the accelerated life test. The devices that have obvious problem in I-L-V characteristics or surface appearance were excluded before the test. Here, the atmospheric temperature and current density were 150°C and about 19 kA/cm^2, respectively. The junction temperature increased due to the self-heating effect. It was calculated from input power and thermal resistance at the operating condi-

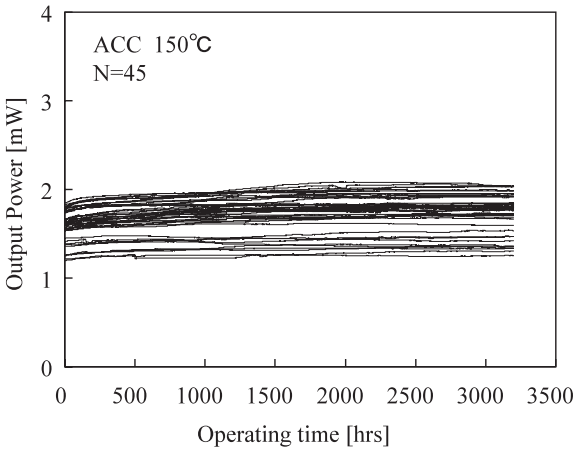

Fig. 4 Output power variation of 45 devices during accelerated life test.

tion [14], which was 208°C. No degradation was observed over 3,000 hours of operating time. The result shows that not only high speed but also high reliability was achieved.

3. Tunnel Junction VCSELs

3.1 Approach for Higher Speed Operation

The main limiting factor of the bandwidths of VCSELs is saturation of relaxation oscillation frequency (fr) against current. The fr can be expressed as follows.

$$fr = \frac{1}{2\pi}\sqrt{\frac{\partial g}{\partial n}\cdot\frac{\Gamma\eta_i(I-I_{th})}{e\cdot S_a\cdot L_{eff}}} \tag{1}$$

Here, $\delta g/\delta n$ is differential gain, Γ is optical confinement factor, η_i is internal quantum efficiency, S_a is area of the active region, and L_{eff} is effective cavity length.

The main cause of fr saturation is presumably decrease of $\delta g/\delta n$ with an increase of current, which is chiefly due to the self-heating effect [15]. By reducing electrical resistance of VCSELs, the self-heating effect can be suppressed and consequently the decrease of $\delta g/\delta n$ can also be suppressed. However, it is difficult to reduce the resistance of conventional oxide-confined VCSELs. Therefore, we tried another structure, a tunnel junction VCSEL (TJ-VCSEL). With this structure, it is possible to reduce the resistance drastically because this structure enables us to omit p-type DBR, which is the main part of the resistance. It is also expected to improve current injection uniformity [16], which may contribute to increase of $\delta g/\delta n$ because current crowding can cause reduction of $\delta g/\delta n$.

According to equation (1), it is also effective to reduce L_{eff} for increase of fr. The L_{eff} includes not only the so-called "cavity length," which is the distance between two DBRs, but also the penetration depth in DBRs. In the case of conventional VCSELs, penetration depth dominates the effective cavity length. Thus, reducing the penetration depth in DBRs is important for reducing the effective cavity length. The penetration depth can be greatly shortened with dielectric layers for DBRs because much higher contrast of refractive index can be achieved compared to semiconductor layers.

From the above reason, we decided to fabricate TJ-VCSELs with dielectric DBRs.

3.2 Type-II Tunnel Junction

A structure with a tunnel junction has mainly been adopted for VCSELs that operate at longer wavelengths than 1.3 μm [17]–[20] because achieving low resistance tunnel junctions for short wavelength VCSELs is difficult, as explained below. Actually, VCSELs with tunnel junction operating at 0.98 μm showed larger resistance than long wavelength VCSELs [21]. Our VCSELs have InGaAs quantum wells as active layers and operate around 1.1 μm, which is a relatively short wavelength. So, achieving good performance with a tunnel junction is not easy.

To solve the trade-off between resistance and optical absorption, we proposed a tunnel junction with a type-II heterostructure [22], [23]. Using the Wentzel-Kramers-Brillouin (WKB) approximation, tunneling probability is represented as

$$Pt \cong \exp\left[-2\int_{x_1}^{x_2}\sqrt{\frac{2m*}{\hbar^2}(E_c-E_f)}dx\right] \tag{2}$$

Here, a one-dimensional model is used. E_c and E_f are the conduction band edge and the Fermi energy level, respectively. x_1 and x_2 are the starting and end points of electron tunneling.

Equation (1) shows that reducing (x_2-x_1) and (E_c-E_f) is important for increasing tunneling probability and achieving low resistance. To reduce (x_2-x_1), high dopant concentration is essential. A low diffusion constant is also needed because dopant diffusion at the p-n interface during crystal growth or device process degrades the tunnel junction, which reduces tunneling probability.

On the other hand, optimizing the band structure of the tunnel junction is important for reducing (E_c-E_f), which is easily done by using semiconductors with low bandgap energy. However, to avoid absorption, the bandgap should not be smaller than the energy of the lasing wavelength. Therefore, it is difficult to achieve a low resistance tunnel junction for short wavelength light that has large energy. For this reason, a structure with a tunnel junction is only adopted for VCSELs that operate at wavelengths longer than 1.3 μm. To solve this problem and apply the tunnel junction structure to our VCSELs that operate around 1.1 μm, we applied a type-II heterojunction. Figure 5 shows an example of an energy band diagram for a type-II tunnel junction. In Figure 5(a), E_{gp} and E_{gn} are the bandgap energy of the p-side and n-side semiconductors, respectively. ΔE_c and ΔE_v are the discontinuity of the conduction band and the valence band, respectively. E_{geff} is the effective bandgap energy of the type-II tunnel junction.

In this structure, $(E_c - E_f)$ at $x = x_1$ becomes E_{geff},

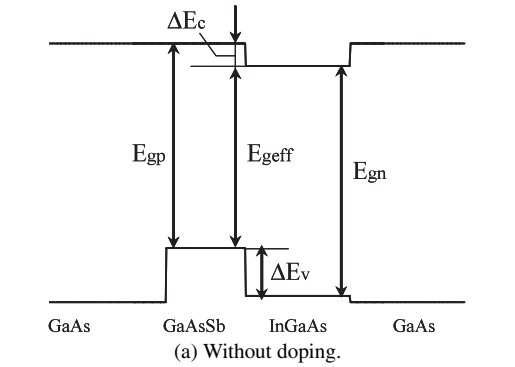

(a) Without doping.

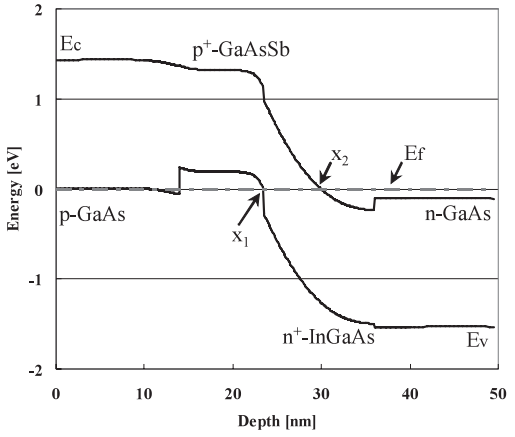

(b)With high-doping.

Fig. 5 Energy band diagram for type-II tunnel junction with p-$GaAsSb_{0.12}$ and n-$In_{0.16}GaAs$ sandwiched by p- and n-type GaAs layers. Active doping concentration of each layer was assumed to be 1.5×10^{20} cm^{-3} for GaAsSb and 5×10^{19} cm^{-3} for InGaAs and 1×10^{19} cm^{-3}, 3×10^{18} cm^{-3} for p- and n-type GaAs, respectively.

which is smaller than E_{gp} and E_{gn}. So, tunneling probability becomes larger than a homojunction or type-I heterojunction.

Even though E_{gp} and E_{gn} are larger than the energy of the lasing wavelength, optical absorption can occur in the heterointerface neighborhood by transition from the valence band edge of the p side to the conduction band edge of the n side. However, the transition needs penetration of the carrier wave function into the bandgap. So its probability, which determines absorption, is not so high. Besides, absorption can be reduced by placing the heterointerface around a standing wave node for negligible small results. This structure also enables smaller built-in potential than homo or type-I tunnel junctions. It leads to reduction of $(x_2 - x_1)$, which also contributes to increasing the tunnel probability.

We chose GaAsSb and InGaAs as p-type and n-type layers, respectively, because they form a type-II heterojunction, as shown in Fig. 5, and dopant concentration higher than GaAs can be achieved. Carbon and silicon were used as p- and n-type dopants, which are suitable for achieving high doping and low diffusion.

With the type-II tunnel junction that consisted of $In_{0.16}Ga_{0.84}As$ and $GaAs_{0.88}Sb_{0.12}$, low specific resistance of

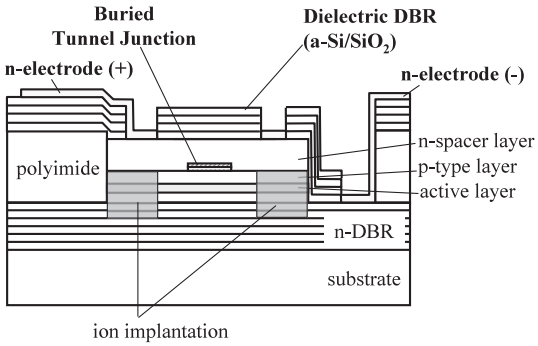

Fig. 6 Schematic of device structure of TJ-VCSEL.

$4 \times 10^{-6}\,\Omega$cm^2 was achieved [23]. The bandgap energies of InGaAs and GaAsSb are larger than the energy of 1.1-μm-wavelength light. Thus, tunnel junction can be adopted for 1.1-μm-range VCSELs. The specific resistance corresponded to a resistance of 14 Ω for a 6-μm aperture diameter, which was much lower than the resistance of conventional oxide-confined VCSELs with identical current aperture. Although not only current apertures but also other parts contribute to the resistances of VCSELs, the resistances of the high-speed VCSELs, which have small apertures, are mainly determined by the resistances around current blocking structures. Thereby, the electrical resistance of VCSELs can be drastically reduced with a tunnel junction structure.

3.3 Device Structure and Fabrication

Figure 6 shows the schematic of the device structure of a TJ-VCSEL. It was fabricated on a Si-doped GaAs substrate by two-step MOVPE. First, the bottom DBR, the active layer and the Type-II TJ were grown. The bottom DBR consisted of n-type GaAs-$Al_{0.9}Ga_{0.1}As$ layers. The active layer was comprised of three $In_{0.3}Ga_{0.7}As$-GaAs (5/10 nm) quantum wells. We added modulation p-doping of 2×10^{18} cm^{-3} in the barrier layers to decrease the nonlinear gain coefficient [24]. The type-II TJ consisted of n-$In_{0.15}Ga_{0.85}As$ (Si $= 5 \times 10^{19}$ cm^{-3}) and p-$GaAs_{0.91}Sb_{0.09}$ ($C = 1.5 \times 10^{20}$ cm^{-3}). Next, we formed the circular TJ apertures using a photolithography technique and wet etching. The diameter of the aperture ranged from 4 μm to 7 μm. Next, oxygen ions were implanted around the TJ to reduce electrical capacitance. We fabricated VCSELs with and without oxygen ion implantation for comparison. Then, the n-type spacer layer was grown on it. After that, the dielectric top DBR that consisted of 3 pairs of amorphous Si (a-Si) layers and SiO_2 layers was deposited. The reflectivity of the top DBR was higher than 99%. As a convenient means of on-wafer measurement, we formed both electrodes on the same side. After the circular mesa was formed with dry etching, the mesa was buried with polyimide to reduce capacitance between the pad electrode and the conducting substrate.

As mentioned in Sect. 3.1, the fabricated structure has smaller L_{eff} compared to conventional oxide-confined VCSELs. Figure 7 shows calculated light intensity distribution

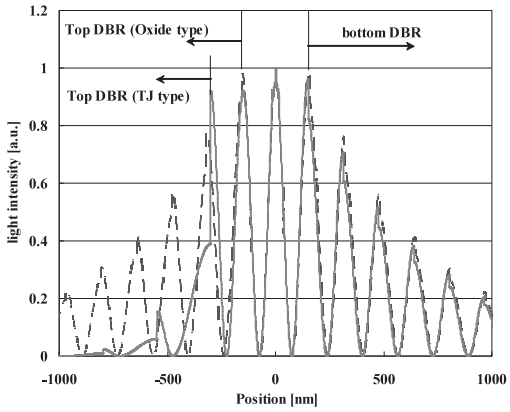

Fig. 7 Calculated light intensity distributions in VCSELs. Solid and dashed lines indicate distribution in TJ-VCSELs and in oxide-confined VCSELs, respectively. 1.5 wavelength cavity was used for TJ-VCSEL, while a one wavelength cavity was used for oxide-confined VCSEL.

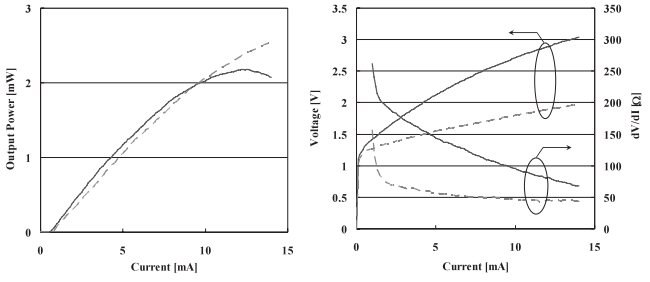

(a) L-I characteristics. (b) V-I and dV/dI-I characteristics.

Fig. 8 L-I and I-V characteristics of TJ-VCSELs with 6-μm aperture diameter at 25°C. Solid and dashed lines indicate characteristics of TJ-VCSELs with/without ion implantation, respectively.

in the TJ-VCSEL. For comparison, calculated results for an oxide-confined VCSEL are also shown. Solid and dashed lines indicate the light intensity distribution of a TJ-VCSEL and the oxide-confined VCSEL, respectively. This time, a 1.5-wavelength cavity was used for the TJ-VCSEL, while a one-wavelength cavity was used for the oxide-confined VCSEL. Thus, the optical length of the TJ-VCSEL cavity is longer than the oxide-confined VCSEL by 0.5 wavelengths. However, penetration depth in the top DBRs in the TJ-VCSEL is about 1.3 wavelengths shorter than the oxide-confined VCSEL [25]. Therefore, in total, the effective cavity length of the TJ-VCSEL is shorter than the oxide-confined VCSEL.

3.4 Characteristics

Figure 8 shows the L-I and I-V characteristics of TJ-VCSELs with a 6-μm aperture diameter at 25°C. The solid and dashed lines indicate TJ-VCSEL characteristics with and without ion implantation, respectively. The threshold current was as low as 0.6 mA and lasing wavelength was 1.09 μm. The VCSEL without ion implantation showed low electrical resistance of around 50 Ω at a bias current of 5 mA. The resistance of 50 Ω is larger than the resistance

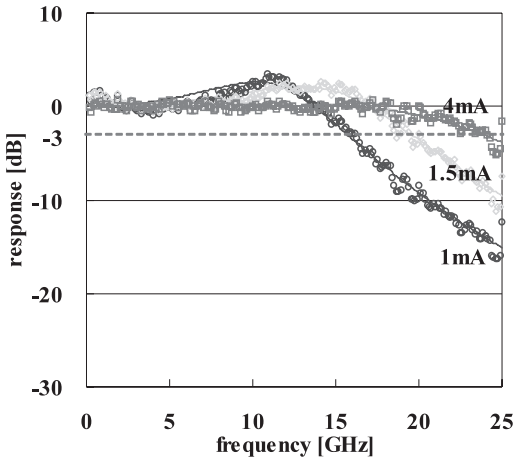

Fig. 9 Small signal modulation response of TJ-VCSEL with 5-μm aperture diameter. Circles are measured data and lines are fitting results.

calculated from the specific resistance of the tunnel junction, which is about 14 Ω for a 6-μm aperture. One reason is the ohmic resistance of the ring electrode on the n-type spacer layer. Another explanation is that the bulk resistance of the n-type spacer layer cannot be negligible. Current is injected from the ring electrode to the tunnel junction by the thin n-type spacer layer. Although the spacer layer is relatively high-doped, it has a certain level of resistance of several to ten ohms because the layer's thickness is only about 0.2 μm.

Besides, the resistance of the tunnel junction in the TJ-VCSEL might be higher than that of the test wafer. In the test wafer, the p-GaAsSb layer was grown on the n-InGaAs layer to fabricate only the tunnel junction on the n-type substrate. On the other hand, in the TJ-VCSEL, since the n-InGaAs layer was grown on the p-GaAsSb layers, this difference of growth sequence may have changed the tunnel junction resistance. The heat history during the n-type spacer layer growth might cause diffusion of the dopants at the tunnel junction interface, which would increase tunnel junction resistance. Still, the resistance was about half that of our oxide-confined VCSELs [9], and we believe that it is the smallest resistance in VCSELs operating at shorter than 1.3 μm for identical current aperture size. On the other hand, VCSEL resistance with ion implantation was higher than the VCSEL without implantation because the profile of the ion implantation was not appropriate and n-DBR resistance in the nonimplanted area was much higher than expected. Consequently, the self-heating effect was not suppressed sufficiently, and the optical power saturated at lower power and lower bias current. This can be improved by optimization of the ion implantation profile.

Next, we measured the modulation response of TJ-VCSELs on-wafer with air coplanar probes. Although the resistance was increased, the RC time constant of the VCSELs with ion implantation was smaller compared to the VCSELs without it. Thus, we used ion implanted TJ-VCSELs for the modulation experiments. Figure 9 shows

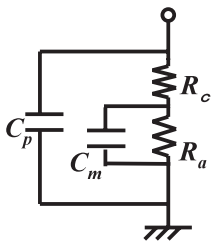

(a) Equivalent circuit.

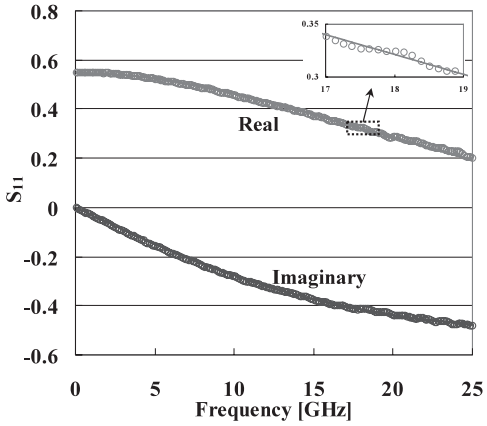

(b) S_{11} parameter versus frequency from model and measured data. Circles are measured data and lines are fitting results. As shown in the inset, they agree well.

Fig. 10 Equivalent circuit and S_{11} data at bias current of 4 mA. Measured data were fitted very well, indicating adequacy of model.

the small-signal modulation response of a TJ-VCSEL with a 5-μm diameter aperture. Figure 5 also shows the fitting curve, which will be explained later. High −3 dB bandwidth of 24 GHz was achieved at a bias current of 4 mA, which is believed to be the highest frequency reported to date for VCSELs.

Next, we derived fr from the measured data as follows. The modulation response of semiconductor lasers can be expressed by the following expression [26]:

$$|M(f)|^2 = \left(\frac{f_r^4}{(f_r^2 - f^2)^2 + (\gamma/2\pi)^2 f^2}\right) \cdot |P(f)|^2 \qquad (3)$$

Here, fr is the relaxation oscillation frequency, γ is the damping rate, and $P(f)$ represents the parasitic circuit effect.

First, we extracted the parameters of a small-signal equivalent circuit for the TJ-VCSELs by fitting the measured data of electrical reflection coefficient S_{11}. Figure 10(a) shows the equivalent circuit that we applied, which is the same circuit for an oxide-confined VCSEL [1]. Figure 10(b) shows the measured S_{11} data at a bias current of 4 mA and the fitting result. The fitting curve agrees with the measured data, which indicates the validity of the equivalent circuit. The estimated values of Ra, Rs, Cm, and Cp were 137.6 Ω, 33.0 Ω, 90 fF, and 22 fF, respectively. Next, the 3-dB frequency of the equivalent circuit model for the TJ-VCSEL driven from a 50-Ω source, that is, $P(f)$ in expression (3), was calculated using those parameters.

Then fr and γ were extracted by fitting expression (3) to the measured small-signal modulation response data.

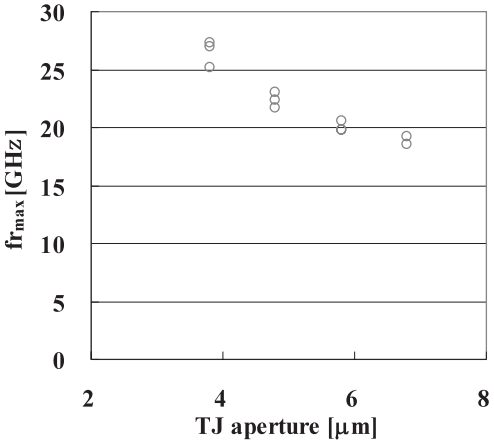

Fig. 11 Maximum relaxation oscillation frequency as a function of apertures.

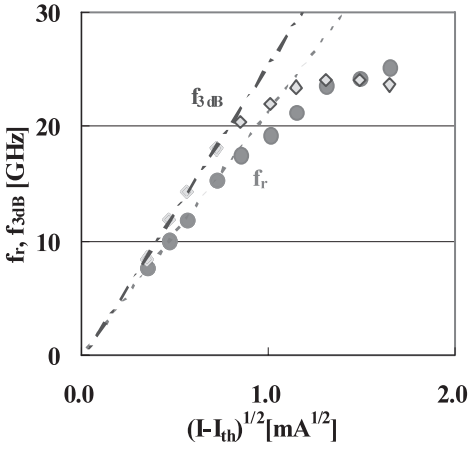

Fig. 12 Dependences of fr and bandwidth on injection current for device with 4-μm current aperture.

As shown in Fig. 9, the measured data are fitted by the above expression well. Therefore, we believe that the fr and γ extracted by this procedure are appropriate.

Figure 11 shows maximum fr as a function of apertures. As the aperture becomes small, fr becomes larger. Very high fr up to 27 GHz was achieved with an aperture diameter of 4 μm. To our knowledge, this is the highest fr for VCSELs. The K-factor was 0.23 ns. A band width of 31 GHz can be achieved without the parasitic circuit effect.

Figure 12 shows the dependences of fr and bandwidth on the injection current for the device with a 4-μm current aperture. The bandwidth increases rapidly at low currents, reaching 20 GHz at a bias current of only 1 mA. The slope of fr against the square root of the current above a threshold (D-factor) and the modulation current efficiency factor (MCEF) for the device below a current of 0.8 mA were as high as 21.3 GHz/$mA^{1/2}$ and 25.0 GHz/$mA^{1/2}$, respectively. Higher D-factor and MCEF can be obtained with smaller aperture size, which was not fabricated this time.

Transmission experiments were carried out under a rate

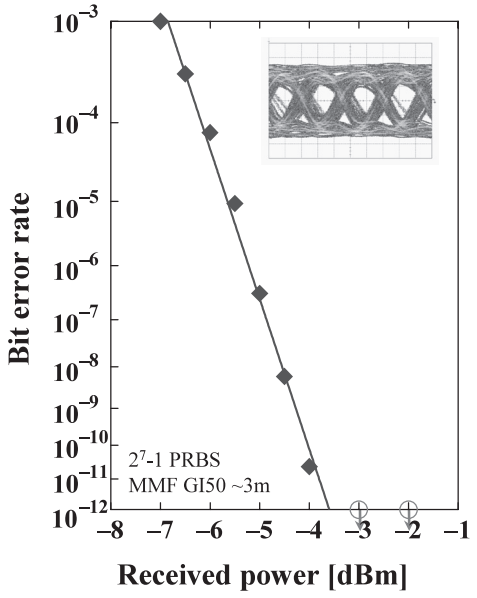

Fig. 13 Measured eye diagrams and bit error rates of the TJ-VCSEL under 40 Gbit/s transmission rate.

of 40 Gbit/s and a pseudorandom bit sequence of $2^7 - 1$ word length. We used a TJ-VCSEL with a 6-μm aperture diameter. We also used the same receiver that was used for transmission experiments of oxide-confined VCSELs in Sect. 2.3 and a graded index 50-μm multi-mode fiber (GI50 MMF). The length of the MMF was about 3 m. Figure 13 shows an eye diagram under a modulation voltage of 0.76 $V_{p\text{-}p}$ and a bias current of 5 mA, where an eye opening can be observed. The extinction ratio was 5.3 dB. Figure 13 also shows the bit error rates (BER) as a function of received optical power under identical conditions as the eye diagram measurement. Our results demonstrate that error-free operation (BER $< 10^{-12}$) was achieved.

This time, we aimed to achieve high relaxation oscillation frequency and high bandwidth by reducing electrical resistance, which leads to the suppression of self-heating effects, and by improving the D-factor. Although the reduction of electrical resistance with a tunnel junction structure was demonstrated, ion implantation increased resistance. Consequently, the self-heating effect was not adequately suppressed. However, high relaxation oscillation frequency and high bandwidth were achieved by significant improvements of the D-factor. Reduction of the effective cavity length was probably one cause of the improvement, but other effects might also have contributed. Further improvement of bandwidth can be achieved by reducing the electrical resistance of ion-implanted TJ-VCSELs with optimization of the implantation profile and the structure of n-type semiconductor DBRs.

4. Conclusions

We have developed InGaAs-based VCSELs operating around 1.1 μm for high-speed optical interconnections. By applying GaAsP barrier layers, temperature characteristics were considerably improved compared to GaAs barrier layers. As a result, 25 Gbps 100°C error-free operation was achieved. These devices also exhibited high reliability. No degradation was observed over 3,000 hours under operation temperature of 150°C and current density of 19 kA/cm^2. We also developed VCSELs with a tunnel junction for higher speed operation. High modulation bandwidth of 24 GHz and a relaxation oscillation frequency of 27 GHz were achieved. 40 Gbps error-free operation was also demonstrated.

Acknowledgments

The authors would like to thank N. Sumihiro, S. Tahara, and H. Kouta for their encouragement throughout the course of this work and T. Yokomatsu and Y. Tarui for their technical assistance.

References

[1] K.L. Lear, V.M. Hietala, H.Q. Hou, J. Banas, B.E. Hammons, J. Zolper, and S.P. Kilcoyne, "High-speed 850 nm oxide-confined vertical cavity surface emitting lasers," Ultrafast Electronics and Optoelectronics 1997 Topical Meeting, Tech. Digest, pp.80–82, 1997.

[2] A.N. AL-Omari and K.L. Lear, "Polyimide-planarized vertical-cavity surface-emitting lasers with 17.0-GHz bandwidth," IEEE Photonics Technol. Lett., vol.16, no.4, pp.969–971, 2004.

[3] P. Pepeljugoski, D. Kuchta, Y. Kwark, P. Pleunis, and G. Kuyt, "15.6-Gb/s transmission over 1 km of next generation multimode fiber," IEEE Photonics Technol. Lett., vol.14, no.5, pp.717–719, 2004.

[4] D.M. Kuchta, P. Pepeljugoski, and Y. Kwark, "VCSEL modulation at 20 Gb/s over 200 m of multimode fiber using a 3.3v SiGe laser driver IC," WA1.2, LEOS Summer Topical Meeting 2001, 2001.

[5] B.M. Hawkins, R.A. Hawthorne, III, J.K. Guenter, J.A. Tatum, and J.R. Biard, "Reliability of various size oxide aperture VCSELs," Proc. 52nd Electron. Components and Technol. Conf., pp.540–550, 2002.

[6] T. Aggerstam, R. Marrcks Von Würtemberg, C. Runnström, and E. Choumas, "Large aperture 850 nm oxide-confined VCSELs for 10 Gb/s data communication," Proc. SPIE, vol.46494, pp.19–25, 2002.

[7] S. Weisser, E.C. Larkins, K. Czotscher, W. Benz, J. Daleiden, I. Esquivias, J. Fleissner, J.D. Ralston, B. Romero, R.E. Sah, A. Schönfelder, and J. Rosenzweig, "Damping-limited modulation bandwidths up to 40 GHz in undoped short-cavity $In_{0.35}Ga_{0.65}As$-GaAs multiple-quantum-well lasers," IEEE Photonics Technol. Lett., vol.8, no.5, pp.608–610, 1996.

[8] R.G. Waters, D.P. Bour, S.L. Yellen, and N.F. Ruggieri, "Inhibited dark-line defect formation in strained InGaAs/AlGaAs quantum well lasers," IEEE Photonics Technol. Lett., vol.2, no.8, pp.531–533, 1990.

[9] K. Fukatsu, K. Shiba, Y. Suzuki, N. Suzuki, T. Anan, H. Hatakeyama, K. Yashiki, and M. Tsuji, "30 Gb/s over 100-m MMFs using 1.1-μm range VCSELs and photodiodes," IEEE Photonics Technol., Lett., vol.20, no.11, pp.909–910, 2007.

[10] Y.-C. Chang, C.S. Wang, and L.A. Coldren, "High-efficiency, high-speed VCSELs with 35 Gbit/s error-free operation," Electron. Lett., vol.43, no.19, pp.1022–1023, 2007.

[11] J.W. Matthews and A.E. Blakeslee, "Defects in epitaxial multilayers: I. Misfit dislocations," J. Cryst. Growth, vol.27, pp.118–125, 1974.

[12] H. Yamaguchi, X. Zhang, K. Ota, M. Nagahara, K. Onabe, Y. Shiraki, and R. Ito, "Photoreflectance study of GaAs/GaAsP strained-barrier quantum well structures," Jpn. J. Appl. Phys.,

vol.32, part 1, no.1B, pp.544–547, 1993.
[13] R.A. Morgan, M.K. Hibbs-Brenner, T.M. Marta, R.A. Walterson, S. Bounnak, E.L. Kalweit, and J.A. Lehman, "200°C, 96-nm wavelength range, continuous-wave lasing from unbonded GaAs MOVPE-grown vertical cavity surface-emitting lasers," Photon. Tech. Lett., vol.7, no.5, pp.441–443, 1995.
[14] P.V. Mena, J.J. Morikuni, S.-M. Kang, A.V. Harton, and K.W. Wyatt, "A simple rate-equation-based thermal VCSEL model," J. Lightwave Technol., vol.17, no.5, pp.865–872, 1999.
[15] K.L. Lear and A.N. Al-Omari, "Progress and issues for high speed vertical cavity surface emitting lasers," Proc. SPIE, 6484-16, 2007.
[16] S. Sekiguchi, T. Miyamoto, T. Kimura, G. Okazaki, F. Koyama, and K. Iga, "Improvement of current injection uniformity and device resistance in long-wavelength vertical-cavity surface-emitting laser," Jpn. J. Appl. Phys., vol.39, part 1, no.7A, pp.3997–4001, 2000.
[17] M. Ortsiefer, R. Shau, F. Mederer, R. Michalzik, J. Rosskopf, G. Bohm, F. Kohler, C. Lauer, M. Maute, and M.-C. Amann, "High-speed modulation up to 10 Gbit/s with 1.55 μm wavelength InGaAsAs VCSELs," Electron. Lett., vol.38, no.20, pp.1180–1181, 2002.
[18] N. Nishiyama, C. Caneau, G. Guryanov, X.S. Liu, M. Hu, and C.E. Zah, "High efficiency long wavelength VCSEL on InP grown by MOCVD," Electron. Lett., vol.39, no.5, pp.437–439, 2003.
[19] D. Feezell, D.A. Buell, and L.A. Coldren, "Continuous-wave operation of all-epitaxial InP-based 1.3 μm VCSELs with 57% differential quantum efficiency," Electron. Lett., vol.41, no.14, pp.803–804, 2005.
[20] J. Boucart, G. Suruceanu, P. Royo, V.I. Iakovlev, A. Syrbu, A. Caliman, A. Mereuta, A. Mircea, C.-A. Berseth, A. Rudra, and E. Kapon, "3.125-Gb/s modulation up to 70°C using 1.3-μm VCSELs fabricated with localized wafer fusion for 10 GBASE LX4 applications," IEEE Photonics Technol. Lett., vol.18, no.4, pp.571–573, 2006.
[21] J.J. Wierer, P.W. Evans, N. Holonyak, Jr., D.A. Kellogg, "Vertical cavity surface emitting lasers utilizing native oxide mirrors and buried tunnel contact junctions," Appl. Phys. Lett., vol.72, no.21, pp.2742–2744, 1998.
[22] T. Anan, Japan Patent Kokai 2002-134835.
[23] N. Suzuki, T. Anan, H. Hatakeyama, and M. Tsuji, "Low resistance tunnel junctions with type-II hetero-structures," Appl. Phys. Lett., vol.88, 231103, 2006.
[24] J.D. Ralston, S. Weisser, I. Esquivias, E.C. Larkins, J. Rosenzweig, P.J. Tasker, and J. Fleissner, "Control of differential gain, nonlinear gain, and damping factor for high-speed application of GaAs-Based MQW lasers," IEEE J. Quantum Electron., vol.29, no.6, pp.1648–1659, 1993.
[25] D.I. Babic and S.W. Corzine, "Analytic expressions for the reflection delay, penetration depth, and absorptance of quarter-wave dielectric mirrors," IEEE J. Quantum Electronics, vol.28, no.2, pp.514–524, 1992.
[26] R. Nagarajan, T. Fukushima, J.E. Bowers, R.S. Geels, and L.A. Coldren, "High-speed InGaAs/GaAs strained multiple quantum well lasers with low damping," Appl. Phys. Lett., vol.58, no.21, p.2326, 1991.

Naofumi Suzuki received the B.E. and M.E. degrees in electrical engineering from Kyoto University, Kyoto, Japan, in 1991 and 1993, respectively. In 1993, he joined NEC Corporation, where he has been engaged in the research and development of semiconductor laser diodes.

Takayoshi Anan received the B.E., M.E. degrees in applied physics from the University of Tokyo, Tokyo, Japan, in 1984 and 1986, respectively. In 1986, he joined the Opto-Electronics Research Laboratories, NEC Corporation, Kawasaki, Japan, where he has been engaged in research and development on semiconductor lasers and its new materials. From 1992 to 1993 he was with Rensselaer Polytechnic Institute, Troy, NY as a visiting researcher.

Hiroshi Hatakeyama was born in Akita prefecture, Japan, on September 9, 1970. He received his B.S. degree and M.E. degree in electronics from Utsunomiya University, Tochigi, Japan in 1993 and 1995, respectively. He joined NEC Corporation in 1995, and is now an assistant manager in the Nano Electronics Research Laboratories, Shiga, Japan. He had been engaged in the development of semiconductor optical amplifiers and tunable laser diodes for optical fiber communication systems. He is a member of the IEEE Lasers and Electro-Optics Society.

Kimiyoshi Fukatsu received M.E. degree in electrical engineering from University of Tokyo in 2000. In 2000, he joined NEC photonic and wireless devices reseach laboratories, Japan. He has been engaged in research and development on optical modules and semiconductor optical devices. His current research is optical devices and modules for optical interconnections at NEC nano electronics research laboratories, Shiga, Japan.

Kenichiro Yashiki was born in Hiroshima, Japan, on May 18, 1969. He received a B.S. in applied physics from the University of Tokyo, Japan. In 1992 he joined NEC Corporation, where he was engaged in research and development of II-VI laser diodes for storage application, and WDM light sources such as wavelength selectable light sources and electroabsorption modulator integrated light sources. He is a member of the Japan Society of Applied Physics (JSAP) and he received a best paper award at the Fifth optoelectronics and communications conference (OECC 2000).

Keiichi Tokutome joined the Opto-Electronics Research Laboratories, NEC Corporation, Tsukuba, Japan, in 1991, where he has been engaged in research and development on semiconductor lasers and its new materials.

Takeshi Akagawa was born in Tokyo, Japan, in 1980. He received the B.E., M.E. degrees in applied physics from Tokyo University of Agriculture and Technology, Tokyo, Japan, in 2003 and 2005, respectively. In 2005, he joined the System Devices Research Laboratories, NEC Corporation, Otsu, Japan, where he has been engaged in research and development on semiconductor lasers.

Masayoshi Tsuji was born in Kumamoto, Japan, in 1964. He received the B.E., M.S., and Ph.D. degrees in electrical and electronic engineering from the Toyohashi University of Technology, Aichi, Japan, in 1987, 1989, and 1999, respectively. In 1989, he joined the NEC Corporation, Kawasaki, Japan. From 1989 to 2000, he had been engaged in research and development of III-V epitaxial growth techniques, InAlGaAs superlattice avalanche photodiodes and high power 0.98 μm lasers for long-wavelength optical communications at Opto-Electronics Research Laboratories, NEC Corporation, Kawasaki (until 1991) and Tsukuba, Japan. From 2003, he has been working on the research of high-speed VCSEL and photo-diode for high-end computing system at Nano-Electronics Research Laboratories, NEC Corporation, Ohtsu. Dr. Tsuji is a member of the Japan Society of Applied Physics.